ADVANCING EARTH AND SPACE SCIENCES

Geophysical Research Letters

RESEARCH LETTER
10.1029/2023GL106649

Key Points:

- Asymmetric flux transport by bottom-up and top-down processes leads to varying flux divergence/convergence (FDC) in the surface layer
- Latent heat and CO_2 fluxes are underestimated when soil is wet and overestimated when dry, but sensible heat flux is always underestimated
- Non-closure of the surface energy balance is regulated by varying FDC and improves for dry soils due to overestimated latent heat flux

Supporting Information:

Supporting Information may be found in the online version of this article.

Correspondence to:

H. Liu,
heping.liu@wsu.edu

Citation:

Liu, H., Liu, C., Huang, J., Desai, A. R., Zhang, Q., Ghannam, K., & Katul, G. G. (2024). Scalar flux profiles in the unstable atmospheric surface layer under the influence of large eddies: Implications for eddy covariance flux measurements and the non-closure problem. *Geophysical Research Letters*, *51*, e2023GL106649. https://doi.org/10.1029/2023GL106649

Received 3 OCT 2023
Accepted 17 DEC 2023

Scalar Flux Profiles in the Unstable Atmospheric Surface Layer Under the Influence of Large Eddies: Implications for Eddy Covariance Flux Measurements and the Non-Closure Problem

Heping Liu[1], Cheng Liu[2], Jianping Huang[3], Ankur R. Desai[4], Qianyu Zhang[1], Khaled Ghannam[5,6], and Gabriel G. Katul[7]

[1]Department of Civil and Environmental Engineering, Washington State University, Pullman, WA, USA, [2]Jiangxi Province Key Laboratory of the Causes and Control of Atmospheric Pollution/School of Water Resources and Environmental Engineering, East China University of Technology, Nanchang, China, [3]Environmental Modeling Center, Lynker, NOAA National Centers for Environmental Prediction, College Park, MD, USA, [4]Department of Atmospheric and Oceanic Sciences, University of Wisconsin-Madison, Madison, WI, USA, [5]Department of Civil and Environmental Engineering, Northeastern University, Boston, MA, USA, [6]Program in Atmospheric and Oceanic Sciences, Princeton University, Princeton, NJ, USA, [7]Department of Civil and Environmental Engineering, Duke University, Durham, NC, USA

Abstract How convective boundary-layer (CBL) processes modify fluxes of sensible (*SH*) and latent (*LH*) heat and CO_2 (F_c) in the atmospheric surface layer (ASL) remains a recalcitrant problem. Here, large eddy simulations for the CBL show that while *SH* in the ASL decreases linearly with height regardless of soil moisture conditions, *LH* and F_c decrease linearly with height over wet soils but increase with height over dry soils. This varying flux divergence/convergence is regulated by changes in asymmetric flux transport between top-down and bottom-up processes. Such flux divergence and convergence indicate that turbulent fluxes measured in the ASL underestimate and overestimate the "true" surface interfacial fluxes, respectively. While the non-closure of the surface energy balance persists across all soil moisture states, it improves over drier soils due to overestimated *LH*. The non-closure does not imply that F_c is always underestimated; F_c can be overestimated over dry soils despite the non-closure issue.

Plain Language Summary Large swirling motions, called large turbulent eddies, efficiently transport water vapor, carbon dioxide, and heat up and down throughout the convective boundary layer (CBL). To what extent scalar fluxes in the atmospheric surface layer (ASL) are modulated by large turbulent eddies from the top of the CBL (i.e., top-down eddies) remains a recalcitrant problem in many fields spanning atmospheric sciences, hydrology, ecology, and climate change. Here, high-resolution computational simulations of the CBL show that scalar fluxes in the ASL linearly change with height across soil wetness conditions largely due to changes in the interactions of top-down processes and bottom-up surface exchange. Such linear height-dependence of the fluxes indicates that reported fluxes from direct turbulent measurements in the ASL are not identical to their sought surface values. As a result, the non-closure of the surface energy balance occurs across all soil moisture conditions but improves as soil becomes dry. CO_2 measured fluxes are underestimated over wet soils and overestimated over dry soils, which has its implication when interpreting CO_2 exchanges from global flux measuring networks utilizing turbulence theories. Height dependence of fluxes, which confirms that the constant flux layer assumption is not routinely satisfied, is a fundamental reason for the non-closure.

1. Introduction

The coupling between land-atmosphere exchange and convective boundary-layer (CBL) processes is increasingly being interrogated (Helbig et al., 2021). Experimental, theoretical, and modeling work has unveiled that fluxes of heat, water vapor, and greenhouse gases (e.g., CO_2, CH_4) in the atmospheric surface layer (ASL) are not only driven by local atmospheric processes but can be subject to non-local contributions originating in the CBL (Khanna & Brasseur, 1997; Gao et al., 2016, 2017; McColl et al., 2016; H. Liu et al., 2021), albeit with varied causes and magnitudes across studies. One consensus that emerges is that interpreting ASL fluxes, typically measured by eddy covariance systems or simulated by land-surface models, necessitates an understanding of how

CBL processes holistically modulate turbulence and fluxes in the ASL (Ghannam et al., 2017; D. Li et al., 2018; Q. Li et al., 2018; Butterworth et al., 2021; H. Liu et al., 2021). This query becomes increasingly pertinent given the substantial role ASL fluxes play in weather and climate modeling across diverse spatial and temporal scales.

The coupling between the ASL and the outer region of the overlying mixed layer (ML) within the CBL is enhanced by the presence of large coherent structures. These structures either initiate at the surface and ascend toward the CBL top (termed ejections or bottom-up) or are driven by entrainment fluxes from the inversion layer (termed sweeps or top-down) (Ghannam et al., 2017; D. Li et al., 2018; H. Liu et al., 2021). In this context, the terminology 'ejections' and 'sweeps' signifies conditioning on positive (ejections) and negative (sweeps) vertical velocity fluctuations only, rather than an analogy to the ejection-sweep cycle commonly studied through the lens of quadrant analysis (Ghannam et al., 2017; Zahn et al., 2022). Nonetheless, these coherent eddies are more energetic than small-scale turbulence, resulting in more effective mixing of scalar quantities throughout the CBL, including the ASL. For instance, sweeping eddies originating near the ML top can impinge on the ASL, causing deviation in ASL turbulence statistics from those predicted by Monin-Obukhov similarity theory (MOST) (Khanna & Brasseur, 1997; Wyngaard, 1982). The temperature similarity function conditioned on sweeps shows a deviation from MOST but follows ML scaling (Q. Li et al., 2018). Conversely, this same function conditioned on ejections remains reasonably predicted by MOST, a feature that is attributed to the sweep-induced potential temperature fluctuations (Q. Li et al., 2018).

In addition to their influence on ASL turbulence, these large eddies regulate turbulent flux transport of scalars within the ASL through their asymmetric flux contributions (D. Li et al., 2018). With increasing instability, the imbalance in flux contributions between ejections and sweeps becomes more pronounced, resulting in the enhanced coupling between the ASL and the overlying ML (Katul et al., 1997; D. Li et al., 2018; Li & Bou-Zeid, 2011; H. Liu et al., 2021). This asymmetry also leads to a breakdown of the gradient-diffusion approximation across a broad range of instability conditions in the CBL (Ghannam et al., 2017). Additionally, the stratification in the free atmosphere influences ASL turbulent quantities under convective conditions (Mellado et al., 2016), linked to the role of sweeps. All these findings underscore the vital role of boundary-layer processes as a whole in regulating turbulent quantities and fluxes in the ASL. The argument of whether and how asymmetric flux transport by sweeps and ejections of large eddies influences and is influenced by variations in flux profiles (i.e., divergence and convergence) for heat, water vapor, and CO_2 in the ASL—commonly assumed as a constant flux layer—has been minimally explored. Furthermore, it remains unclear what implications such changes in flux profiles hold for the non-closure of the surface energy balance, and whether this non-closure necessarily corresponds to underestimated CO_2 flux in the ASL by the same eddy covariance system that reports underestimates in sensible and latent heat fluxes.

To address this gap, a series of large eddy simulations (LESs) are performed for horizontally homogeneous, quasi-stationary CBL flows over a flat domain covered with uniform short grasses under various soil moisture conditions (Text S1 in Supporting Information S1).

2. LES Model and Configurations

The LES model used here was developed by the National Center for Atmospheric Research (Moeng, 1984; Patton et al., 2005; Sullivan et al., 1996) and coupled with a land-surface model (Huang et al., 2009, 2011). The salient features of the LES model and its setup are presented in Text S2 in Supporting Information S1. Following the setup in C. Liu et al. (2021), the simulation domain size is set to $5.0 \times 5.0 \times 1.92$ km, with a grid spacing of 12.5 m $\times$ 12.5 m $\times$ 5 m and grid number of $400 \times 400 \times 384$ in the x, y, and z directions, respectively. These settings result in a boundary-layer height to grid spacing ratio exceeding 100, which is sufficient for CBL turbulence (Sullivan & Patton, 2011). In all the simulations, a constant incoming solar radiation of 700 W m^{-2} is imposed, and a zero geostrophic wind is set (i.e., shear-free CBL). The surface roughness length remains fixed at 0.1 m, which is commensurate to a grass field of 1 m in height, while the surface albedo is fixed at 0.2. Changes in Bowen ratio β, which is defined as the ratio of surface sensible heat flux (SH_0) to surface latent heat flux (LH_0) (i.e., $\beta = SH_0/LH_0$), are caused by variations in the partitioning of the available energy ($R_{n0}-G_0$, where R_{n0} is the surface net radiation and G_0 is the ground heat flux) into SH_0 and LH_0 through altering the soil moisture parameter f_n in the LSM (Huang et al., 2009) (Table S1 in Supporting Information S1).

All simulations are initiated with profiles of potential temperature (θ), specific humidity (q), and CO_2 mixing ratio (C) that are uniform in the horizontal directions across the domain (Text S2, Figure S1 in Supporting

Information S1). The settings for the initial profiles of θ, q, and C, as shown in Figure S1 in Supporting Information S1, are similar to those adopted in previous LES studies based on the data collected during the 1994 field campaign of the Boreal Ecosystem-Atmosphere Study (BOREAS) (e.g., Huang et al., 2009; C. Liu et al., 2021). The boundary layer heights (z_i), initially set to 960 m for all these six CBL cases, reach their respective quasi-steady state values ranging from 1,062 m to 1,154 m as β increases from 0.51 to 1.91 (Table S1 in Supporting Information S1). The 1-hr averaged simulated results are analyzed only after the turbulent kinetic energy averaged across the domain reaches a quasi-steady state.

3. Results and Discussion

3.1. Changes in Flux Profiles in the CBL With Varying Soil Moisture

Figures 1a–1c show the normalized fluxes of kinematic sensible heat ($\overline{w'\theta'}/\overline{w'\theta'}_0$), water vapor ($\overline{w'q'}/\overline{w'q'}_0$), and CO_2 ($\overline{w'C'}/\overline{w'C'}_0$), respectively, across the six soil moisture conditions as a function of z/z_i. Here and throughout, w represents the instantaneous vertical velocity component along the wall-normal z axis, where $z = 0$ denotes the ground. The primed variables represent turbulent fluctuations around their respective time-averaged states. All fluxes to be analyzed in this section are domain-averaged across all the horizontal grid points after time-averaged fluxes are calculated for each grid point (Text S2 in Supporting Information S1).

As expected, $\overline{w'\theta'}/\overline{w'\theta'}_0$ in the stationary CBL exhibits a linear decrease with increasing z/z_i (indicating flux divergence) for all soil moisture conditions (i.e., all the β values). The slopes of the $\overline{w'\theta'}/\overline{w'\theta'}_0$ profiles exhibit a minute increase as β increases due to decreasing soil moisture (Figure 1a). Conversely, the $\overline{w'q'}/\overline{w'q'}_0$ decreases linearly with z/z_i under the two wet soil moisture conditions ($\beta = 0.51$ and 0.60), signifying flux divergence (Figure 1b). For the remaining four relatively dry soil moisture conditions (i.e., $\beta = 0.74$, 0.90, 1.32, and 1.91), $\overline{w'q'}/\overline{w'q'}_0$ increases linearly with z/z_i (illustrating flux convergence). The slopes of $\overline{w'q'}/\overline{w'q'}_0$ increase with the increasing β from 0.51 to 0.60, and then become positive values that decrease with the increasing β from 0.74 to 1.91. Similar to $\overline{w'q'}/\overline{w'q'}_0$, $\overline{w'C'}/\overline{w'C'}_0$ decreases linearly with z/z_i as β increases from 0.51 to 0.90 under the four wet soil moisture cases (indicating flux divergence). It then increases linearly with z/z_i as β continues to increase for the remaining two dry soil moisture cases with β values of 1.32 and 1.91 (signifying flux convergence) (Figure 1c). Linear dependences of $\overline{w'\theta'}/\overline{w'\theta'}_0$, $\overline{w'q'}/\overline{w'q'}_0$, and $\overline{w'C'}/\overline{w'C'}_0$ on z/z_i have been reported in previous studies and simply indicate good statistical convergence of time and planar averaging of LES outcomes to text-book expectations (Andre et al., 1978; Ek & Holtslag, 2004; Ghannam et al., 2017; Huang et al., 2008, 2009, 2011; Mellado et al., 2017; Stull, 1988). However, the underlying mechanisms regulating changes in the flux divergence and convergence in the CBL across varying β values have remained relatively unexplored.

3.2. Changes in Flux Profiles in the CBL Regulated by Asymmetric Contributions of Top-Down and Bottom-Up Processes

We now investigate whether the changes in flux profiles (i.e., changes in divergence and convergence) with the varying β values, as depicted by the LES results in the preceding section, can be elucidated by the theoretical arguments outlined below. According to the linear nature of the mean conservation equations, scalar fluxes in the CBL can be quantified as a linear superposition of their respective top–down and bottom–up contributions and given by Wyngaard and Brost (1984) and Huang et al. (2008),

$$\overline{w's'} = \overline{w's'}_0\left(1 - \frac{z}{z_i}\right) + \overline{w's'}_{z_i}\frac{z}{z_i}, \tag{1}$$

where s denotes a generic scalar. Re-organization of Equation 1 yields,

$$\frac{\overline{w's'}}{\overline{w's'}_0} = 1 - (1 - \alpha)\left(\frac{z}{z_i}\right). \tag{2}$$

Equation 2 indicates that $\frac{\overline{w's'}}{\overline{w's'}_0}$ exhibits a linear dependency on z/z_i and this normalized dependency can be quantified by a single parameter—the entrainment ratio for the scalar flux (α). This α is defined as the ratio of the

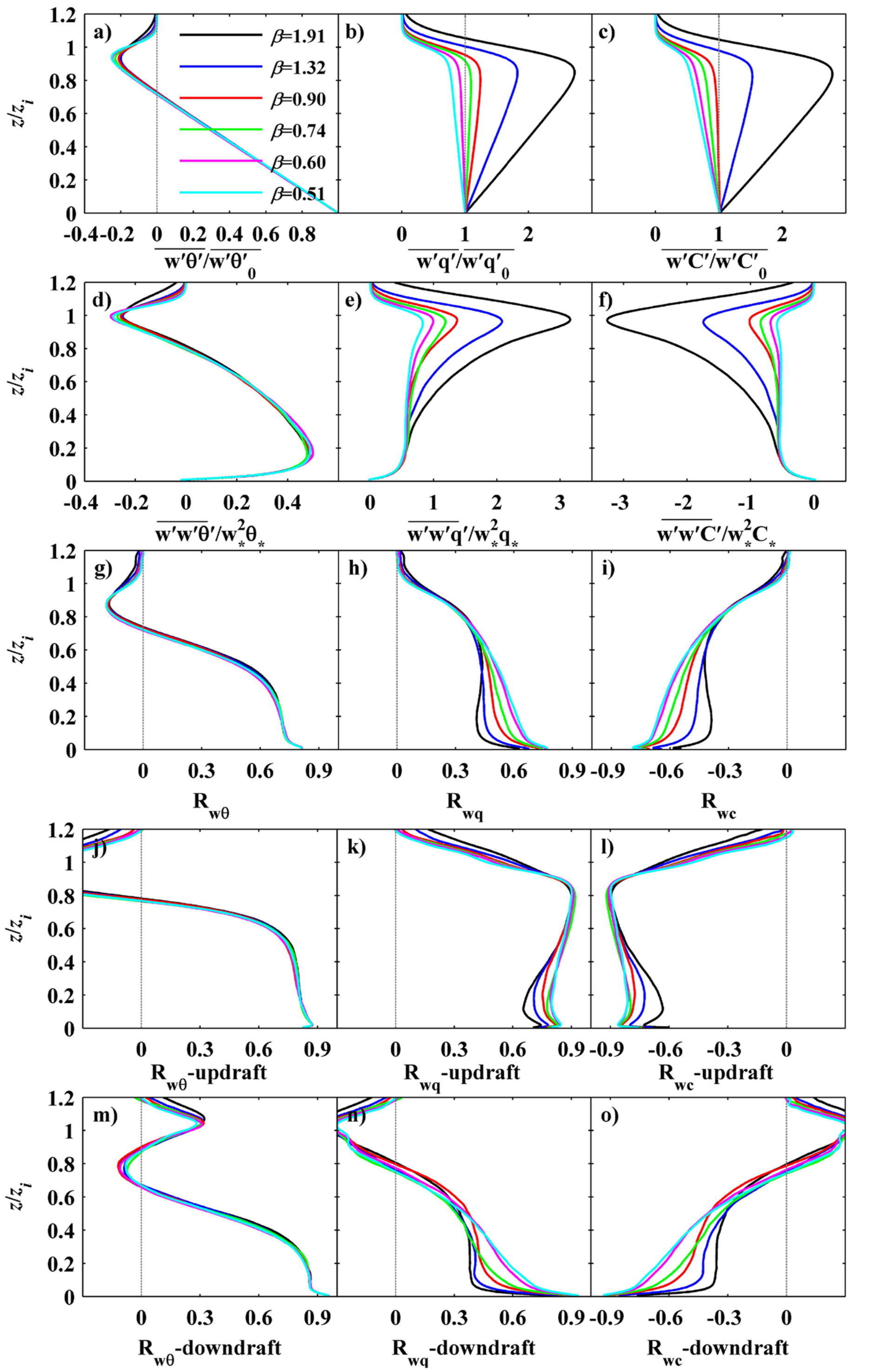

Figure 1. Vertical profiles of the normalized (a) kinematic heat flux ($\overline{w'\theta'}/\overline{w'\theta'}_0$), (b) water vapor flux ($\overline{w'q'}/\overline{w'q'}_0$), and (c) CO_2 flux ($\overline{w'C'}/\overline{w'C'}_0$), third-order moments of (d) $\overline{w'w'\theta'}/w_*^2\theta_*$, (e) $\overline{w'w'q'}/w_*^2q_*$, (f) $\overline{w'w'C'}/w_*^2C_*$ and (g) $R_{w\theta}$, (h) R_{wq}, and (i) R_{wc}, the updraft components of (j) $R_{w\theta}$, (k) R_{wq}, and (l) R_{wc}, and the downdraft components of (m) $R_{w\theta}$, (n) R_{wq}, and (o) R_{wc} under different soil moisture conditions. Note that the flux transport efficiencies for sensible heat, latent heat, and CO_2 fluxes are expressed as $R_{w\theta} = \frac{\overline{w'\theta'}}{\sigma_w\sigma_\theta}$, $R_{wq} = \frac{\overline{w'q'}}{\sigma_w\sigma_q}$, and $R_{wc} = \frac{\overline{w'c'}}{\sigma_w\sigma_c}$, respectively. Note that both $\overline{w'C'}$ at any heights in the CBL and $\overline{w'C'}_0$ are negative for the six cases in the model domain covered with grass, making the $\overline{w'C'}/\overline{w'C'}_0$ values positive through the CBL. $w_* = \left[\frac{gz_i}{\bar{\theta}}\overline{w'\theta'}_0\right]^{1/3}$, $\theta_* = \frac{\overline{w'\theta'}_0}{w_*}$, $q_* = \frac{\overline{w'q'}_0}{w_*}$, and $C_* = \frac{\overline{w'C'}_0}{w_*}$ represent the convective velocity scale, temperature scale, humidity scale, and CO_2 scale, respectively. g is the gravitational acceleration.

top-down entrainment flux of the corresponding scalar by sweeps at the CBL top to the bottom-up surface scalar exchange (i.e., $\alpha = \overline{w's'}_{z_i}/\overline{w's'}_0$).

As $\overline{w'\theta'}_0$ increases with decreasing soil moisture (i.e., increasing β), ejections driven by the increased $\overline{w'\theta'}_0$ become energetic and intrude upward into the upper CBL, evidenced by the positive vertical velocity in Figure 2. This process enhances sweeps driven by entrainment, resulting in the enhanced downward impingement on the ASL, ultimately leading to an enhanced coupling of the ASL with the CBL, as indicated by the negative vertical velocity in Figure 2. As β increases, however, the reduced $\overline{w'q'}_0$ and $\overline{w'C'}_0$ from the surface lead to the weakened bottom-up transfer of these two scalars, causing them progressively to retreat to lower levels in the CBL (Figure 2b vs. 2h for q; 2f vs. 2l for C). Consequently, the top-down transfer of all the scalars by large eddies is substantially enhanced as β increases, whereas the bottom-up transfer of water vapor and CO_2 weakens, while heat is enhanced, though both the top-down and bottom-up processes are dynamically enhanced (Figure 2a vs. 2i). These differing features are further reflected by the increased magnitudes of the turbulent flux transport (i.e., $\overline{w'w'\theta'}/w_*^2\theta_*$, $\overline{w'w'q'}/w_*^2q_*$, and $\overline{w'w'C'}/w_*^2C_*$) in the top part of the CBL as well as the increased magnitudes of $\overline{w'w'\theta'}/w_*^2\theta_*$ and the decreased $\overline{w'w'q'}/w_*^2q_*$ and $\overline{w'w'C'}/w_*^2C_*$ in the bottom part of the CBL (Figures 1d–1f; Figure S2 in Supporting Information S1). To be clear, the flux divergences arise from the mean continuity equation whereas the aforementioned turbulent flux transport terms arise from an entirely different budget - the turbulent scalar flux budgets. Large eddies can also be discerned by the horizontal distribution patterns of the vertical winds and scalars at $z = 80$ m (approximately $z/z_i = 0.08$), which become more organized at higher β and exert stronger effects on fluxes (Figures S3 and S4 in Supporting Information S1).

As β increases from 0.51 to 1.91, $\overline{w'\theta'}_0$ and $\overline{w'\theta'}_{z_i}$ increase by 87% and 78%, respectively. While $\overline{w'q'}_0$ and $\overline{w'C'}_o$ are reduced by 50% and 75%, respectively, $\overline{w'q'}_{z_i}$ and $\overline{w'C'}_{z_i}$ increase by 129% and 75%, respectively. Consequently, α for $\overline{w'\theta'}$, $\overline{w'q'}$, and $\overline{w'C'}$ increases by 23%, 271%, and 453%, respectively (Table S1 in Supporting Information S1). The increased α for $\overline{w'\theta'}$ is attributed to the more disproportionately increased bottom-up flux than the increased top-down flux, signifying changes in the asymmetry in flux contributions by the bottom-up and top-down processes with the varying β values. The increased α for $\overline{w'q'}$ and $\overline{w'C'}$ with increasing β carries two implications. First, the top-down processes are progressively strengthened, leading to the enhanced contributions of the top-down induced scalars and their fluxes to the respective scalars and fluxes in the lower part of the CBL. This enhancement is reflected in the overall decreased flux transport efficiencies for water vapor and CO_2 (i.e., R_{wq} and R_{wc}) (Figures 1g–1i), with more significant effects by sweeps (i.e., R_{wq}-downdraft and R_{wc}-downdraft) than ejections (i.e., R_{wq}-updraft and R_{wc}-updraft) (Figures 1j–1l vs. Figures 1m–1o; Figure S2 in Supporting Information S1). This enhancement is also evidenced by the larger changes in R_{wq}-downdraft and R_{wc}-downdraft than R_{wq}-updraft and R_{wc}-updraft in the ASL with increasing β. Using Figure 1n as an example, entrained air masses carrying negative R_{wq}-downdraft from the top of the CBL are brought down by downdrafts to the lower section of the CBL, resulting in a reduction of R_{wq}-downdraft. Consequently, the enhanced top-down processes contribute to a decrease in R_{wq}-downdraft as β increases. Second, the increased α indicates that flux contributions by sweeps and ejections to $\overline{w'q'}$ and $\overline{w'C'}$ become increasingly asymmetric across the CBL, including the ASL, as β increases. Moreover, the changes in this asymmetry in flux contributions are the primary process that regulates the changes in the dimensionless slopes of the flux profiles with varying β, as quantified by (1-α) in Equation 2. The α for $\overline{w'\theta'}$ experiences small variations with the increasing β (i.e., flux divergence), resulting in subtle changes in the slopes of the $\overline{w'\theta'}/\overline{w'\theta'}_0$ profiles as soil moisture decreases. However, the large increases in α for $\overline{w'q'}$ and $\overline{w'C'}$ from less than 1 to greater than 1 as β increases cause $\overline{w'q'}/\overline{w'q'}_0$ and $\overline{w'C'}/\overline{w'C'}_0$ to decrease with z/z_i when their respective α is less than 1 (i.e., flux divergence) and increase with z/z_i when their respective α is great than 1 (i.e., flux convergence). Changes in the fluxes obtained from LES are consistent with those predicted by Equation 2 when using the scalar specific α values in Table S1 in Supporting Information S1 as expected.

3.3. Changes in the Non-Closure Linked to Changes in Varying Flux Divergence and Convergence in the ASL

Given that the LES model calculates fluxes as covariance, the modeled fluxes at any levels in the ASL, defined as the bottom 10% of the CBL, can be interpreted as equivalent to those that would be measured by an eddy covariance system positioned above the surfaces (Inagaki et al., 2006; Kanda et al., 2004; Zhou et al., 2018). Therefore, eddy covariance fluxes in the ASL can be interpreted as underestimated if the measured fluxes at a specific level (i.e.,

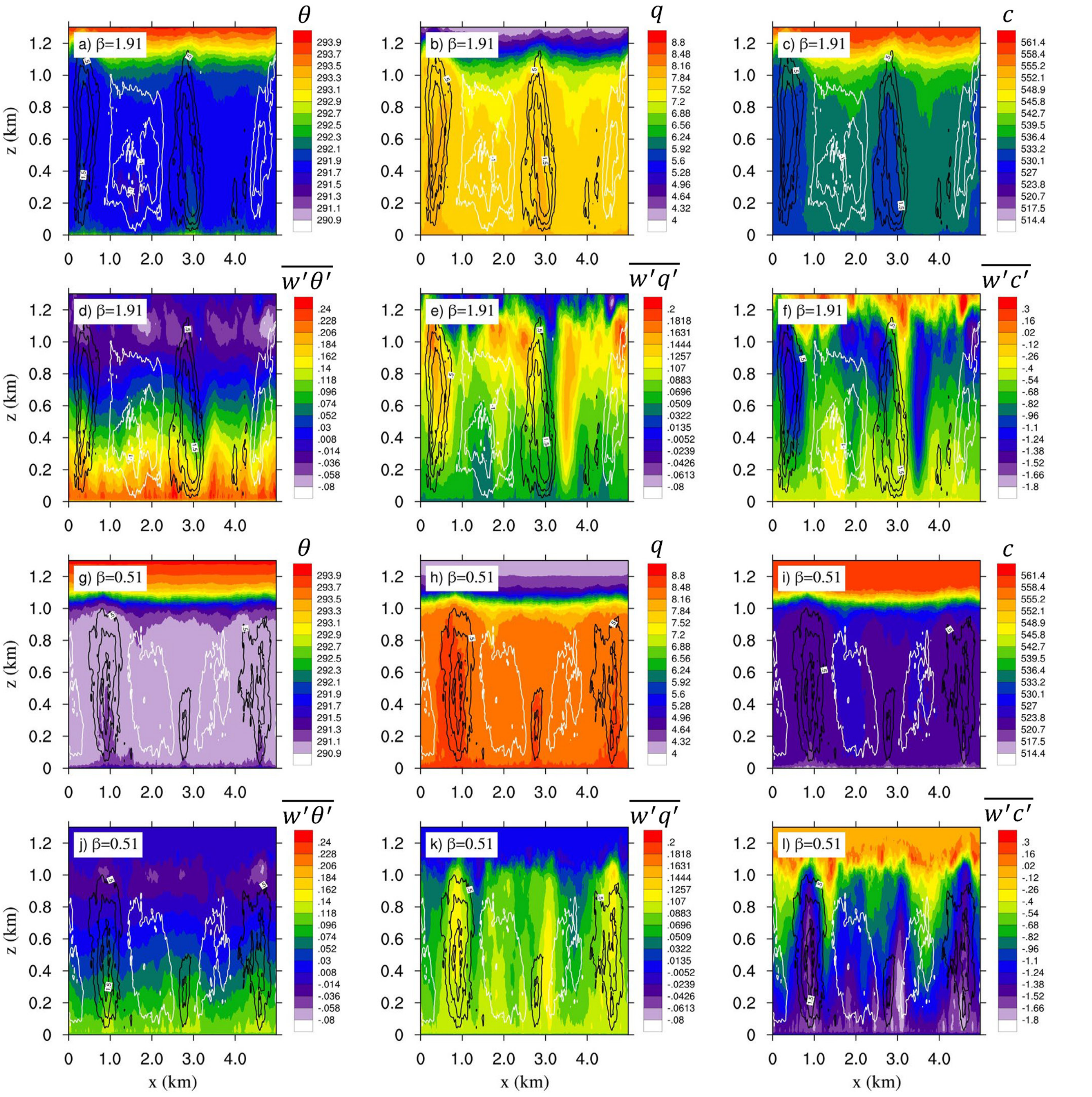

Figure 2. *x–z* cross-sections of (a, g) potential temperature (θ, K), (b, h) specific humidity (q, g/kg), (c, i) CO_2 mixing ratio (c, mg/kg), (d, j) $\overline{w'\theta'}$, (e, k) $\overline{w'q'}$, (f, l) $\overline{w'c'}$ for $\beta = 0.51$ and $\beta = 1.91$. The black contour lines represent positive vertical velocity (>0.5 m s^{-1}) and the white contour lines represent negative vertical velocity (<−0.5 m s^{-1}). As β increases, overshooting thermals induced by the enhanced vertical velocity invade into the top of the CBL, leading to enhanced entrainments. As a result, the enhanced mixing of scalars by ejections and sweeps is illustrated respectively by the enhanced ascending and descending plume-liked patterns in (a), (b), and (c), as compared with (g), (h), and (i), respectively. The enhanced transport of scalars by ejections and sweeps is also reflected by the increased scalar fluxes across the CBL, as depicted by the enhanced ascending and descending plume-liked patterns of each scalar flux in (d), (e), and (f), as compared with (j), (k), and (i), respectively.

$\overline{w'\theta'}$, $\overline{w'q'}$, and $\overline{w'C'}$) are less than their corresponding "true" surface interfacial fluxes (i.e., $\overline{w'\theta'}_0$, $\overline{w'q'}_0$, and $\overline{w'C'}_0$), and vice versa. Equation 2 suggests that for z/z_i<<1, the turbulent fluxes represent their surface value provided $|\alpha|$ is not too large when compared to unity. Across the ASL, the linear decrease in $\overline{w'\theta'}/\overline{w'\theta'}_0$ with height indicates that *SH* measured by eddy covariance systems are consistently underestimated regardless of soil

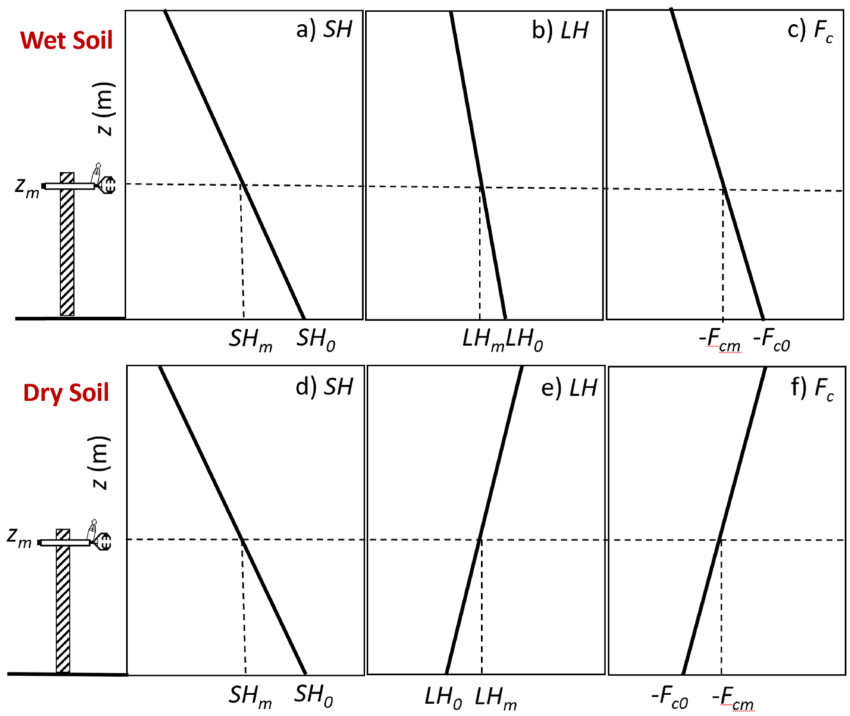

Figure 3. Schematic showing changes in scalar flux profiles with soil moisture in the unstable ASL, as adopted from the LES results in this study. Under wet soil conditions (a, b, c), fluxes of sensible heat (SH_m), latent heat (LH_m), and CO_2 (F_{cm}) measured by the eddy covariance system at a certain height (z_m) in the unstable ASL are smaller than their corresponding surface fluxes (i.e., SH_0, LH_0, and $-F_{c0}$). Therefore, $SH_m < SH_0$, $LH_m < LH_0$, and $-F_{cm} < -F_{c0}$. Under dry soil conditions, SH_m is underestimated (d) but both LH_m and F_{cm} are overestimated (e, f). Therefore, $SH_m < SH_0$, $LH_m > LH_0$, and $-F_{cm} > -F_{c0}$. $CR = \frac{SH_m + LH_m}{SH_0 + LH_0} < 1$ for both the wet soil and dry soil cases. Note that CO_2 fluxes over this grass surface are negative (i.e., $F_c < 0$) at any heights in the CBL for all the six cases so that $-F_c$ is always greater than zero at any heights in the CBL by adding a negative sign to F_c.

moisture conditions; whereas the linearly decreasing and increasing $\overline{w'q'}$ profiles indicates that *LH* measured by eddy covariance systems are underestimated and overestimated for the two wettest and the four driest soil cases, respectively (Figure 3; Figure S5 in Supporting Information S1). Note that the non-dimensionalized fluxes in Figure S5 in Supporting Information S1 also support these conclusions.

Next, how the combinations of underestimated SH and underestimated/overestimated LH under different soil moisture conditions contribute to changes in the non-closure is analyzed. Equation SE3 in Supporting Information S1 (i.e., $CR = (SH + LH)/(SH_0 + LH_0)$ in Text S3 in Supporting Information S1) states that the surface energy balance is closed (i.e., $CR = 1$) when the summation of the measured SH and LH at a specific height in the ASL is equal to the summation of their "true" surface fluxes (i.e., $SH_0 + LH_0$). The analysis here focuses on the time-averaged fluxes from a virtual tower at $z = 40$ m (approximately $z/z_i = 0.04$) in the center grid of the homogeneous domain to explore the non-closure problem (De Roo & Mauder, 2018; Xu et al., 2020). Note that the "true" surface fluxes are obtained as the time-averaged fluxes over the domain to address possible footprint issues. Our results indicate that the mean *CR* for all the cases from the virtual tower at $z = 40$ m is 0.8, suggesting that eddy covariance measurements in the ASL underestimate the land-surface fluxes by 20% across the varying soil moisture conditions. Specifically, the *CR* from the virtual tower is 0.71 when averaged for the two wettest cases and increases to 0.90 when averaged for the two driest soil cases, indicating improved closure over drier soils. These findings are consistent with previous experimental evidence that *CR* from eddy covariance flux towers is generally larger under dry soil conditions than under wet soil conditions (e.g., wetlands), as noted in the relation between *CR* and precipitation (Stoy et al., 2013), though the underlying mechanistic causes for this improvement in *CR* under dry soil conditions were not previously reported. Nevertheless, the relations between *CR* and β have yielded inconsistent results (Wilson et al., 2002).

In the subsequent discussion, horizontally domain-averaged fluxes at 40 m from Figure 1 and Figure S5 in Supporting Information S1 are used to draw general conclusions. In dry soil conditions (i.e., high β), the overestimated *LH* (i.e., the *LH* flux convergence with $\overline{w'q'} > \overline{w'q'}_0$) compensates the underestimated *SH* (the *SH* flux convergence), leading to an increased *CR* at $z = 40$ m (Figure S5 in Supporting Information S1). The underestimated *SH* accounts for over 75% of the *CR*, and its contribution slightly increases with β, whereas *LH* contributes less than 25%, with its contribution decreasing with β (Figure S5 in Supporting Information S1). Therefore, this study provides a mechanistic explanation, elucidating that the overestimated *LH* due to the flux convergence under high β is the primary factor explaining the increased *CR* for dry soils despite the further underestimated *SH*.

The distinct linear dependences of $\overline{w'\theta'}$ and $\overline{w'q'}$ with height prompt an inquiry into how the non-closure changes with height under varying soil moisture conditions (but at preset free atmospheric states). The LES results indicate that the *CR* linearly decreases with height for all the soil moisture cases (Figure S5g in Supporting Information S1), though such a relation shows considerable variability when using the *CR* from the virtual tower. The slopes of the linearly decreased *CR* diminish as soil moisture decreases, indicating the progressively improved closure with height as β increases primarily because the overestimated $\overline{w'q'}$ outpaces the underestimated $\overline{w'\theta'}$. Furthermore, *CR* is consistently less than 1, even with the overestimated $\overline{w'q'}$ (i.e., $\overline{w'q'} > \overline{w'q'}_0$) for the two driest soil cases.

The widely reported non-closure issue, which is a persistent challenge in micro-meteorology, carries significant implications for trace gas flux measurements. It has prompted debates within the flux measurement community, particularly regarding whether this non-closure implies potential underestimation of CO_2 fluxes $\left(F_c = \overline{w'C'}\right)$ by the same eddy covariance systems that are considered to underestimate *SH* and *LH* (Foken et al., 2011; Gao et al., 2019). The decreased and increased $\overline{w'C'}$ profiles indicate that F_c measured by eddy covariance measurements in the ASL is underestimated for the two wettest cases with the lowest *CR* and overestimated for the four dries cases with the highest *CR* (Figure S5 in Supporting Information S1), ranging from by −1% at $\beta = 0.51$ to 9% at $\beta = 1.91$. When averaged across the six cases, F_c at $z = 40$ m is overestimated by 2%, despite the existence of the non-closure. In summary, this study reveals that CO_2 fluxes are underestimated under wet soil conditions and overestimated under dry soil conditions irrespective of the persistent non-closure (for the imposed free atmospheric states here). Based on these findings (i.e., Figure 1 and Figure S5 in Supporting Information S1), Figure 3 provides a schematic outlining the flux divergence and convergence in the ASL and their implications for eddy covariance flux measurements and the non-closure problem.

4. Conclusions

Under steady-state and horizontally homogeneous conditions, the LES results converge to theoretical expectations from the mean scalar continuity equations that flux profiles vary linearly with height for *SH*, *LH*, and F_c in the CBL as soil moisture levels change (represented by changes in β). These changes in the flux height-dependences are regulated by interplay between land-surface (bottom-up) and boundary-layer (top-down) processes facilitated by large eddies. As soil moisture decreases, *SH* at the surface increases, intensifying surface thermal forcing. Consequently, thermally induced eddies (i.e., ejections) bolster the entrainment from the top of the ABL through top-down eddies (i.e., sweeps), enhancing the coupling between the land-surface and boundary-layer processes. Changes in asymmetric transport of fluxes by sweeps and ejections modify (and are modified by) the slopes of the flux profiles as β increases, resulting in changes in flux divergence/convergence with soil moisture in the ASL even over this horizontally homogeneous landscape. Consequently, such changes in flux divergence and convergence have significant implications for fluxes measured or reported at various heights in the ASL that are underestimated or overestimated, respectively, as compared with the "true" surface fluxes. Specifically, *SH* in the ASL is consistently underestimated across all the β conditions, whereas *LH* and F_c are underestimated under wet soil conditions with low β and overestimated under dry soil conditions with high β (Figure 3). As a result, the non-closure occurs across all the soil moisture conditions, but the closure improves with drier soil over which latent flux convergence occurs. The non-closure does not necessarily imply that F_c in the ASL is always underestimated; instead, F_c is overestimated over dry soils where non-closure exists (Figure 3). Therefore, changes in the degrees of the non-closure are linked to variations in flux divergence/convergence in the ASL. These findings also imply that a Bowen ratio preserving correction would lead to erroneous adjustments to *SH*, *LH*, and F_c.

The constant flux layer assumption requires constant normalized flux profiles, a concept previously discussed (Wyngaard, 2010). However, its implications for the non-closure problem have not been explored. This assumption implies that flux gradients typically vary by less than 10% in the ASL. Nevertheless, if each of *SH* and *LH* varies 10% with height, the combined effect can potentially result in a 20% variation in the sum of *SH* and *LH* across the ASL, which may explain the widely observed non-closure of 20% in the flux measurement community. The LES results for the convective boundary layer suggest that the non-closure problem is largely linked to a failure of the constant flux layer assumption, which necessitates further studies or improve eddy covariance measurement or calculation approaches. The study also highlights the emerging needs in flux measurements to understand how boundary-layer processes impact ASL exchanges and fluxes in a fully coupled ABL system.

Data Availability Statement

According to the AGU publications Data Policy, the data used in this paper are deposited at Zenodo (Liu et al., 2023).

Acknowledgments
We thank Dr. Jiening Liang for her constructive comments. H. Liu acknowledges support by National Science Foundation (NSF-AGS-2325687 and NSF-AGS-1853050). C. Liu acknowledges support by the National Natural Science Foundation of China (42105088). A. R. Desai acknowledges support from NSF-AGS-1822420 and NSF-2313772. G. G. Katul acknowledges support from the US National Science Foundation (NSF-AGS-2028644) and the U.S. Department of Energy (DE-SC0022072).

References

Andre, I.-C., De Moor, G., Lacarrère, P., & du Vachat, R. (1978). Modeling the 24-hour evolution of the mean and turbulent structures of the planetary boundary layer. *Journal of the Atmospheric Sciences*, *35*(10), 1861–1883. https://doi.org/10.1175/1520-0469(1978)035<1861:mtheot>2.0.co;2

Butterworth, B. J., Desai, A. R., Metzger, S., Townsend, P. A., Schwartz, M. D., Bertram, T. H., et al. (2021). Connecting land-atmosphere interactions to surface heterogeneity in CHEESEHEAD19. *Bulletin of the American Meteorological Society*, *102*(2), E421–E445. https://doi.org/10.1175/BAMS-D-19-0346.1

De Roo, F., & Mauder, M. (2018). The influence of idealized surface heterogeneity on virtual turbulent flux measurements. *Atmospheric Chemistry and Physics*, *18*(7), 5059–5074. https://doi.org/10.5194/acp-18-5059-2018

Ek, M. B., & Holtslag, A. A. M. (2004). Influence of soil moisture on boundary layer cloud development. *Journal of Hydrometeorology*, *5*(1), 86–99. https://doi.org/10.1175/15257541(2004)005<0086:IOSMOB>2.0.CO;2

Foken, T., Aubinet, M., Finnigan, J. J., Leclerc, M. Y., Mauder, M., & Paw U, K. T. (2011). Results of a panel discussion about the energy balance closure correction for trace gases. *Bulletin of the American Meteorological Society*, *92*(4), ES13–ES18. https://doi.org/10.1175/2011bams3130.1

Gao, Z., Liu, H., Katul, G. G., & Foken, T. (2017). Non-closure of the surface energy balance explained by phase difference between vertical velocity and scalars of large atmospheric eddies. *Environmental Research Letters*, *12*(3), 034025. https://doi.org/10.1088/1748-9326/aa625b

Gao, Z., Liu, H., Missik, J. E. C., Yao, J., Huang, M., Chen, X., et al. (2019). Mechanistic links between underestimated CO2 fluxes and non-closure of the surface energy balance in a semi-arid sagebrush ecosystem. *Environmental Research Letters*, *14*(4), 044016. https://doi.org/10.1088/1748-9326/ab082d

Gao, Z., Liu, H., Russell, E. S., Huang, J., Foken, T., & Oncley, S. P. (2016). Large eddies modulating flux convergence and divergence in a disturbed unstable atmospheric surface layer. *Journal of Geophysical Research: Atmospheres*, *121*(4), 1475–1492. https://doi.org/10.1002/2015JD024529

Ghannam, K., Duman, T., Salesky, S. T., Chamecki, M., & Katul, G. G. (2017). The non-local character of turbulence asymmetry in the convective atmospheric boundary layer. *Quarterly Journal of the Royal Meteorological Society*, *143*(702), 494–507. https://doi.org/10.1002/qj.2937

Helbig, M., Gerken, T., Beamesderger, E., Baldocchi, D. D., Banerjee, T., Biraud, S. C., et al. (2021). Integrating continuous atmospheric boundary layer and tower-based flux measurements to advance understanding of land-atmosphere interactions. *Agricultural and Forest Meteorology*, *307*, 108509. https://doi.org/10.1016/j.agrformet.2021.108509

Huang, J., Lee, X., & Patton, E. G. (2008). A modelling study of flux imbalance and the influence of entrainment in the convective boundary layer. *Boundary-Layer Meteorology*, *127*(2), 273–292. https://doi.org/10.1007/s10546-007-9254-x

Huang, J., Lee, X., & Patton, E. G. (2009). Dissimilarity of scalar transport in the convective boundary layer in inhomogeneous landscapes. *Boundary-Layer Meteorology*, *130*(3), 327–345. https://doi.org/10.1007/s10546-009-9356-8

Huang, J., Lee, X., & Patton, E. G. (2011). Entrainment and budgets of heat, water vapor, and carbon dioxide in a convective boundary layer driven by time-varying forcing. *Journal of Geophysical Research*, *116*(D6), D06308. https://doi.org/10.1029/2010JD014938

Inagaki, A., Letzel, M., Raasch, S., & Kanda, M. (2006). Impact of surface heterogeneity on energy imbalance: A study using LES. *Journal of the Meteorological Society of Japan. Ser. II*, *84*(1), 187–198. https://doi.org/10.2151/jmsj.84.187

Kanda, M., Inagaki, A., Letzel, M. O., Raasch, S., & Watanabe, T. (2004). LES study of the energy imbalance problem with eddy covariance fluxes. *Boundary-Layer Meteorology*, *110*(3), 381–404. https://doi.org/10.1023/B:BOUN.0000007225.45548.7a

Katul, G., Kuhn, G., Schieldge, J., & Hsieh, C.-I. (1997). The ejection-sweep character of scalar fluxes in the unstable surface layer. *Boundary-Layer Meteorology*, *83*(1), 1–26. https://doi.org/10.1023/A:1000293516830

Khanna, S., & Brasseur, J. G. (1997). Analysis of Monin–Obukhov similarity from large-eddy simulation. *Journal of Fluid Mechanics*, *345*, 251–286. https://doi.org/10.1017/S0022112097006277

Li, D., & Bou-Zeid, E. (2011). Coherent structures and the dissimilarity of turbulent transport of momentum and scalars in the unstable atmospheric surface layer. *Boundary-Layer Meteorology*, *140*(2), 243–262. https://doi.org/10.1007/s10546-011-9613-5

Li, D., Katul, G. G., & Liu, H. (2018). Intrinsic constraints on asymmetric turbulent transport of scalars within the constant flux layer of the lower atmosphere. *Geophysical Research Letters*, *45*(4), 2022–2030. https://doi.org/10.1002/2018GL077021

Li, Q., Gentine, P., Mellado, J. P., & Mccoll, K. A. (2018). Implications of nonlocal transport and conditionally averaged statistics on Monin-Obukhov similarity theory and Townsend's attached eddy hypothesis. *Journal of the Atmospheric Sciences*, *75*(10), 3403–3431. https://doi.org/10.1175/JAS-D-17-0301.1

Liu, C., Liu, H., Huang, J., & Xiao, H. (2021). Varying partitioning of surface turbulent fluxes regulates temperature-humidity dissimilarity in the convective atmospheric boundary layer. *Geophysical Research Letters*, *48*(21), e2021GL095836. https://doi.org/10.1029/2021GL095836

Liu, H., Gao, Z., & Katul, G. G. (2021). Non-closure of surface energy balance linked to asymmetric turbulent transport of scalars by large eddies. *Journal of Geophysical Research: Atmospheres*, *126*(7), e2020JD034474. https://doi.org/10.1029/2020JD034474

Liu, H., Liu, C., Huang, J., Desai, A. R., Zhang, Q., Ghannam, K., & Katul, G. G. (2023). Scalar flux profiles in the unstable atmospheric surface layer under the influence of large eddies: Implications for eddy covariance flux measurements and the non-closure problem [Dataset]. Zenodo. https://doi.org/10.5281/zenodo.8130814

McColl, K. A., Katul, G. G., Gentine, P., & Entekhabi, D. (2016). Mean-velocity profile of smooth channel flow explained by a cospectral budget model with wall-blockage. *Physics of Fluids*, *28*(3), 035107. https://doi.org/10.1063/1.4943599

Mellado, J., Puche, P. M., & van Heerwaarden, C. C. (2017). Moisture statistics in free convective boundary layers growing into linearly stratified atmospheres. *Quarterly Journal of the Royal Meteorological Society*, *143*(707), 2403–2419. https://doi.org/10.1002/qj.3095

Mellado, J. P., van Heerwaarden, C. C., & Garcia, J. R. (2016). Near-surface effects of free atmosphere stratification in free convection. *Boundary-Layer Meteorology*, *159*(1), 69–95. https://doi.org/10.1007/s10546-015-0105-x

Moeng, C. H. (1984). A large-eddy-simulation model for the study of planetary boundary-layer turbulence. *Journal of the Atmospheric Sciences*, *41*(13), 2052–2062. https://doi.org/10.1175/1520-0469(1984)041<2052:ALESMF>2.0.CO;2

Patton, E. G., Sullivan, P. P., & Moeng, C. H. (2005). The influence of idealized heterogeneity on wet and dry planetary boundary layers coupled to the land surface. *Journal of the Atmospheric Sciences*, *62*(7), 2078–2097. https://doi.org/10.1175/JAS3465.1

Stoy, P. C., Mauder, M., Foken, T., Marcolla, B., Boegh, E., Ibrom, A., et al. (2013). A data-driven analysis of energy balance closure across FLUXNET research sites: The role of landscape scale heterogeneity. *Agricultural and Forest Meteorology*, *171–172*, 137–152. https://doi.org/10.1016/j.agrformet.2012.11.004

Stull, R. B. (1988). *An introduction to boundary layer meteorology*. Kluwer Academic Publishers.

Sullivan, P. P., McWilliams, J. C., & Moeng, C. H. (1996). A grid nesting method for large-eddy simulation of planetary boundary-layer flows. *Boundary-Layer Meteorology*, *80*(1), 167–202. https://doi.org/10.1007/BF00119016

Sullivan, P. P., & Patton, E. G. (2011). The effect of mesh resolution on convective boundary layer statistics and structures generated by large-eddy simulation. *Journal of the Atmospheric Sciences*, *68*(10), 2395–2415. https://doi.org/10.1175/JASD-10-05010.1

Wilson, K., Goldstein, A., Falge, E., Aubinet, M., Baldocchi, D., Berbigier, P., et al. (2002). Energy balance closure at FLUXNET sites. *Agricultural and Forest Meteorology*, *113*(1–4), 223–243. https://doi.org/10.1016/s0168-1923(02)00109-0

Wyngaard, J. C. (1982). In D. K. Lilly & T. Gal-Chen (Eds.), *Lectures on the planetary boundary layer. Mesoscale meteorology—theory, observations and models* (pp. 603–650). D. Reidel.

Wyngaard, J. C. (2010). *Turbulence in the atmosphere*. Cambridge University Press.

Wyngaard, J. C., & Brost, R. A. (1984). Top-down and bottom-up diffusion of a scalar in the convective boundary layer. *Journal of the Atmospheric Sciences*, *41*(1), 102–112. https://doi.org/10.1175/1520-0469(1984)041<0102:TDABUD>2.0.CO;2

Xu, K., Sühring, M., Metzger, S., Durden, D., & Desai, A. R. (2020). Can data mining help eddy-covariance see the landscape? A large-eddy simulation study. *Boundary-Layer Meteorology*, *176*(1), 85–103. https://doi.org/10.1007/s10546-020-00513-0

Zahn, E., Bou-Zeid, E., Good, S. P., Katul, G. G., Thomas, C. K., Ghannam, K., et al. (2022). Direct partitioning of eddy-covariance water and carbon dioxide fluxes into ground and plant components. *Agricultural and Forest Meteorology*, *315*, 108790. https://doi.org/10.1016/j.agrformet.2021.108790

Zhou, Y., Li, D., Liu, H., & Li, X. (2018). Diurnal variations of the flux imbalance over homogeneous and heterogeneous landscapes. *Boundary-Layer Meteorology*, *1–26*.

References From the Supporting Information

Foken, T. (2008). The energy balance closure problem: An overview. *Ecological Applications*, *18*(6), 1351–1367. https://doi.org/10.1890/06-0922.1

Mauder, M., Foken, T., & Cuxart, J. (2020). Surface-energy-balance closure over land: A review. *Boundary-Layer Meteorology*, *9*(8), 1–32. https://doi.org/10.1007/s10546-020-00529-6

Oncley, S., Foken, T., Vogt, R., Kohsiek, W., DeBruin, H. A. R., Bernhofer, C., et al. (2007). The energy balance experiment EBEX-2000. Part I: Overview and energy balance. *Boundary-Layer Meteorology*, *123*(1), 1–28. https://doi.org/10.1007/s10546-007-9161-1